

1 **Future projections of daily haze conducive and clear weather conditions over the North**
2 **China Plain using a Perturbed Parameter Ensemble**

3 Shipra Jain^{1,2}, Ruth M. Doherty¹, David Sexton³, Steven Turnock^{3,4}, Chaofan Li⁵, Zixuan
4 Jia¹, Zongbo Shi⁶, Lin Pei⁷

5 ¹School of GeoSciences, The University of Edinburgh, Edinburgh, United Kingdom

6 ²Centre for Climate Research Singapore (CCRS), Singapore

7 ³Met Office Hadley Centre, Exeter, United Kingdom

8 ⁴University of Leeds Met Office Strategic (LUMOS) Research Group, School of Earth and
9 Environment, University of Leeds, UK

10 ⁵Center for Monsoon System Research, Institute of Atmospheric Physics, Chinese Academy of
11 Sciences, China

12 ⁶School of Geography, Earth and Environmental Sciences, University of Birmingham,
13 Birmingham, United Kingdom

14 ⁷Institute of Urban Meteorology, China Meteorological Administration, Beijing, China

15 ~~Shipra Jain¹, Ruth M. Doherty¹, David Sexton², Steven Turnock^{2,3}, Chaofan Li⁴, Zixuan Jia¹,~~
16 ~~Zongbo Shi⁵, Lin Pei⁶~~

17 ~~¹School of GeoSciences, The University of Edinburgh, Edinburgh, United Kingdom~~

18 ~~²Met Office Hadley Centre, Exeter, United Kingdom~~

19 ~~³University of Leeds Met Office Strategic (LUMOS) Research Group, School of Earth and~~
20 ~~Environment, University of Leeds, UK~~

21 ~~⁴Center for Monsoon System Research, Institute of Atmospheric Physics, Chinese Academy of~~
22 ~~Sciences, China~~

23 ~~⁵School of Geography, Earth and Environmental Sciences, University of Birmingham,~~
24 ~~Birmingham, United Kingdom~~

25 ~~⁶Institute of Urban Meteorology, China Meteorological Administration, Beijing, China~~

26
27 **Corresponding Author:** Shipra Jain (Shipra.Jain@ed.ac.uk)

53 **Abstract**

54 We examine past and future changes in both winter haze and clear weather conditions over the
55 North China Plain (NCP) using a Perturbed Parameter Ensemble (PPE) and elucidate the
56 influence of model physical parameterizations on these future projections for the first time. We
57 use a large-scale meteorology-based Haze Weather Index (HWI) with values >1 as a proxy for
58 haze conducive weather and $\text{HWI} < -1$ for clear weather conditions over the NCP. The PPE
59 generated using the UK Met Office HadGEM-GC3 model shows that under a high-emission
60 (RCP8.5) scenario, the frequency of haze conducive weather ($\text{HWI} > 1$) is likely to increase
61 whereas the frequency of clear weather ($\text{HWI} < -1$) is likely to decrease in future, with a growing
62 influence of climate change over the 21st century. However, Nevertheless, a change of opposite
63 sign with lower magnitude in the frequencies, though less likely, is also possible. In future, the
64 frequency of haze conducive weather for a given winter can be as much as ~ 3.5 times higher
65 than the frequency of clear weather over the NCP. ~~The future frequencies~~ More frequent of haze
66 conducive weather ($\text{HWI} > 1$) during winter over the NCP is found to be ~~are~~ associated with
67 ~~changes in zonal-mean mid-tropospheric winds and the vertical temperature gradient over the~~
68 ~~NCP~~ an enhanced warming of the troposphere and weaker north-westerlies in the mid-
69 troposphere over the NCP. We also examined the changes in the interannual variability of the
70 haze conducive and clear weather, and find no marked changes in the variability of future
71 periods. We find a clear influence of model physical parametrizations on climatological mean
72 frequencies for both haze conducive and clear weather. For mid to late 21st century (2033-
73 2086), parametric effect can explain up to $\sim 80\%$ variance in climatological mean frequencies
74 of PPE members. ~~Therefore,~~ This shows that the different model physical parameterizations
75 lead to a different evolution of model's mean climate, particularly towards the end of the 21st
76 century. Therefore, ~~adds uncertainty in the future projections of haze conducive weather it is~~
77 desirable to consider the PPE in addition to the initialized and multimodel ensembles for a more

Formatted

Formatted

~~comprehensive range of plausible future projections. in addition to the internal variability. We also find a growing influence of anthropogenic climate change on future mean frequencies of haze conducive and clear weather over the 21st century suggesting climate change can exacerbate the haze conducive weather and reduce the clear weather conditions in future over the NCP.~~

83

84 **1. Introduction**

85 Over the last decade, a number of severe haze episodes (several days or longer) were
86 reported over the North China Plain (NCP) during boreal winter (December-January-February,
87 DJF). In January 2013, unprecedented PM_{2.5} levels exceeding 450 µg m⁻³ were observed over
88 the NCP (Wang et al., 2014a; Wang et al., 2014b; Zhang et al., 2018; Zhang et al., 2013).
89 Similar events were also observed in November-December 2015 when the PM_{2.5} concentrations
90 reached as high as 1000 µg m⁻³ in Beijing and caused the first-ever ‘red alert’ for severe air
91 pollution (Liu et al., 2017; Zhang et al., 2017). In December 2016, around 25% of the land area
92 of China was covered with severe haze for around one week (Yin and Wang, 2017). These
93 severe haze events adversely impacted public health including mortality, visibility, and
94 ultimately the economy of the country (Bai et al., 2007; Chen and Wang, 2015; Kan et al.,
95 2012; Kan et al., 2007; Wang et al., 2006; Xu et al., 2013; Hong et al., 2019).

96 Previous research has shown that the persistence of severe haze for days during winters
97 over the NCP occurred due to the combined effect of local and regional high pollutant
98 emissions and stagnant meteorological conditions (Li et al., 2018; He et al., 2016; Jia et al.,
99 2015; Pei et al., 2018; Zhang et al., 2021). The normal winter meteorological conditions over
100 the NCP are characterized by northwesterly flow near the surface through to the mid-
101 troposphere associated with the East Asian winter monsoon circulation (Fig. 1a and 1b; also

102 see An et al., 2019; Chen and Wang, 2015; Li et al., 2016; Renhe et al., 2014; Xu et al., 2006).
103 The northwesterly winds support the intrusion of relatively clean air from the high latitudes to
104 the NCP and therefore ventilate this region (Xu et al., 2006). However, during the severe haze
105 episodes, the ~~near-surface~~lower tropospheric (~850 hPa) northwesterlies appear to be weaker
106 than normal and the mid-tropospheric trough was reported to be shallower and shifted
107 northwards – collectively leading to a weaker than normal northwesterly flow and reduced
108 horizontal transport of air pollutants from the NCP (Fig. 2a-b). In addition to changes in
109 horizontal winds, the vertical temperature gradient between the lower and upper troposphere
110 over the NCP can influence the vertical dispersion of the pollutants. A warmer than normal
111 temperature ~~near the surface~~in the lower troposphere (~850 hPa), accompanied with colder
112 temperature in the upper troposphere (~200 hPa), would enhance the thermal stability and
113 reduce the atmospheric mixing leading to the build-up of the atmospheric pollutants over this
114 region (Fig. 2; also see Hou and Wu, 2016; Sun et al., 2014; Wang et al., 2014a; Zhang et al.,
115 2018; Cai et al., 2018). The planetary boundary layer height is also found to be suppressed
116 during extreme haze events leading to accumulation of pollutants, notably PM_{2.5} concentrations
117 (Liu et al., 2018; Petäjä et al., 2016), due to an increase in moisture, reduced vertical mixing
118 and dispersion which aids aerosol growth during high haze events over the NCP (An et al.,
119 2019; Tie et al., 2017).

120 On a daily scale, past studies have examined the changes in haze conducive weather
121 conditions over China under climate change scenarios using large-scale meteorology-based
122 indexes. For example, Cai et al. (2017) have used four key variables, i.e. meridional wind at
123 850 hPa (V_{850}), zonal wind at 500 hPa (U_{500}), temperatures at 850 hPa (T_{850}) and 250 hPa (T_{250})
124 pressure levels to calculate a meteorology-based daily Haze Weather Index (HWI). They have
125 projected a ~50% increase in the frequency of winter haze conducive weather conditions,
126 similar to the January 2013 event, over Beijing in the future (2050-2099) as compared to the

127 historical (1950-1999) period under the RCP8.5 scenario using 15 CMIP5 models. Using the
128 HWI, Liu et al. (2019) projected a 6-9% increase in the winter haze frequency under 1.5° and
129 2° global warming, respectively based on 20 CMIP5 models whereas Qiu et al. (2020)
130 projected a relatively high increase of 21% and 18% in severe winter haze episodes under 1.5°
131 and 2° global warming, respectively using an ensemble of climate simulations from the
132 Community Earth System Model 1 (CESM1) (Kay et al., 2015). Callahan and Mankin (2020)
133 also used specific humidity, V_{850} , T_{850} and temperatures at 1000 hPa to examine the haze
134 favourable meteorology for Beijing, and found a 10-15% increase in winter haze conducive
135 weather in CMIP5 multimodel and CESM large ensemble under 3° warming. These authors
136 have also emphasized a large influence of internal variability in addition to anthropogenic
137 forcing on future haze conducive weather over Beijing.

138 In addition to the large-scale meteorology based indexes, several other stagnation
139 indices based on regional or local meteorological variables have also been used to determine
140 the influence of anthropogenic climate change on haze conducive weather for China as well as
141 global regions. Using minimum monthly mean wind speeds averaged over northwestern
142 Europe, Vautard et al. (2018) suggested a potential increase in the frequency of stagnant
143 conditions conducive to air pollution over northwest Europe; however, their results were
144 sensitive to models used for the analysis. Horton et al. (2014) have used thresholds for the daily
145 mean near-surface (10-m) wind speeds, mid-tropospheric (500 hPa) temperatures and
146 accumulated precipitation to calculate the Air Stagnation Index (ASI) under RCP8.5 scenario
147 using 15 CMIP5 models. They found an increase in air stagnation occurrence events leading to
148 poor air quality by up to ~40 days per year over a majority of the tropics and sub-tropics. Han
149 et al. (2017) examined indicators of haze pollution potential (e.g. horizontal transport, wet-
150 deposition, ventilation conditions) using three regional climate simulations and projected a
151 higher probability of haze pollution risk over the Beijing-Tianjin-Hebei region under the

152 RCP4.5 scenario. Garrido-Perez et al. (2021) took a different approach as compared to
153 analysing probabilistic projections and used the ASI to generate stagnation storylines, i.e.
154 plausible and physically consistent scenarios of stagnation changes based on the response of
155 remote drivers under climate change forcing, for Europe and the United States (US).

156 While most studies indicate an increase in the haze conducive weather over China, a
157 few studies also find little impact of climate change on future projections of haze (Shen et al.,
158 2018; Pendergrass et al., 2019), which could partly arise due to the under-sampling of internal
159 variability associated uncertainty in their projections (Callahan and Mankin, 2020), as well as
160 model-to-model differences. Hence, there is a large uncertainty as to how haze conducive
161 weather conditions may change in the future and these depend on haze metrics or underlying
162 processes considered for future projections.

163 In order to account for the uncertainty in the future projections (e.g. of large-scale
164 circulation) particularly at the regional scale (Hawkins and Sutton, 2012; Deser et al., 2012;
165 Deser et al., 2014), it is desirable to use an ensemble of climate change simulations. Whilst a
166 multimodel ensemble, e.g. CMIP5 or CMIP6, is commonly used for climate change studies,
167 several other studies have also emphasised the use of an initialised ensemble or Perturbed
168 Parameter Ensemble (PPE) from a single model to assess the uncertainties and obtain a
169 comprehensive range of possible future climate realisations for the same emission scenario for
170 a given model (Knutti et al., 2010). All three methodologies have different advantages. For
171 instance, using multiple models allows us to sample structural uncertainty in future projections,
172 which cannot be sampled using a single model. On the other hand, using an initialised ensemble
173 from a single model allows us to sample a broader range of internal variability, which is often
174 under-sampled in a multimodel ensemble. The advantage of using the PPE over the initialised
175 or multimodel ensemble is that it not only accounts for internal variability but also model
176 uncertainty arising due to the different settings of the physical parameterisations in a single

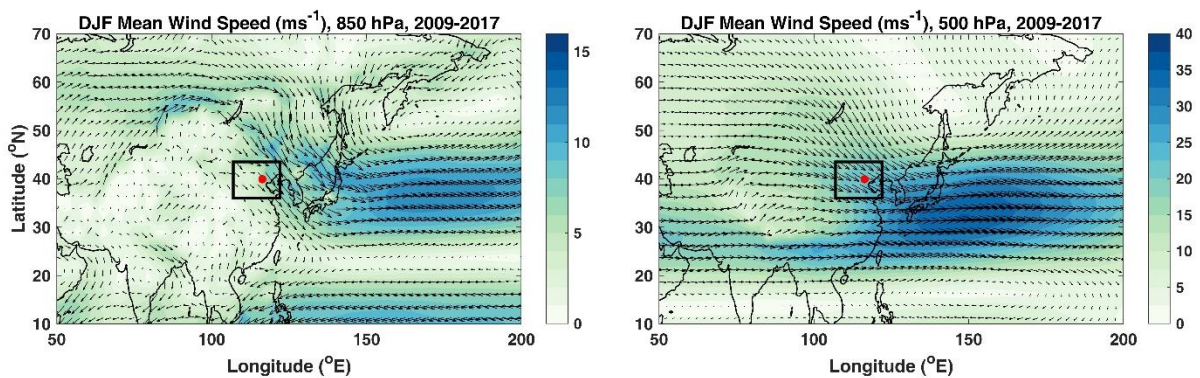
177 model. Both multimodel ensemble and initialised ensemble from a single model have been
178 used to assess the future winter haze conducive conditions over Beijing. In this paper, we use
179 a PPE generated using the UK's Met Office HadGEM-GC3 model to assess for the first time
180 the impact of both model physical parameterisations and anthropogenic climate change on
181 future daily haze conducive weather conditions.

182 In this paper, our focus is on the daily haze conducive and clear weather conditions
183 over the NCP under a fixed high-emission scenario (RCP8.5). For this purpose, we use the
184 HWI proposed by Cai et al. (2018) as past research studies have shown a robust correlation
185 between the HWI, which is a large-scale meteorology based index, and haze conducive weather
186 for Beijing in China. Whilst Cai et al. (2018) originally proposed the HWI for Beijing, the
187 index is based on changes in large-scale meteorology over the NCP and thus offers a good
188 potential as the indicator of haze conducive weather over the NCP. One potential advantage of
189 using the HWI for future projections, as opposed to a regional or local air stagnation index, is
190 that the general circulation models generally simulate large-scale meteorology reasonably well
191 as compared to local or regional meteorology. Therefore, we expect the future projections of
192 clear or haze conducive weather provided using the HWI to be less uncertain than projections
193 provided using regional stagnation indexes.

194 The HWI uses four meteorological variables as stated above, but Cai et al. (2018) have
195 also examined the impact of the inclusion of more weather variables, such as geopotential
196 height, boundary layer thickness and local stratification instability, in the HWI and did not find
197 any significant differences in the performance of the HWI. Therefore, we use the same
198 variables and methodology as Cai et al (2018) to calculate the HWI and provide future
199 projections of haze conducive and clear weather using the HWI. However, our analysis is based
200 on an underlying assumption that the large-scale meteorological conditions, which are used as

201 a basis for the HWI, will have a similar influence on the air quality of the NCP in the future
202 climate as for present-day climate.

203 In this paper, we first examine the application of the HWI as a proxy for haze conducive
204 and clear weather over NCP for the current climate using a suite of observations (Section 3).
205 We then provide the projections of the haze conducive (HWI >1) and clear weather (HWI <-
206 1) frequency over NCP for the historical and future period. We assess the impact of model
207 physical parametrisations and anthropogenic climate change on the frequencies (Section 4).
208 We also analyse the changes in the interannual variance of the frequency of haze conducive
209 and clear weather conditions for the future periods as compared to the historical period (Section
210 5). Finally, we assess the impact of parametric effect and anthropogenic climate change on
211 trends in haze conducive and clear weather occurrence over the 21st century (Section 6). Details
212 of data and methods used in this paper are provided in the next section.



214 **Figure 1** Average wind speed at (a) 850 hPa and (b) 500 hPa pressure level. The red dot
215 represents the location of Beijing and black rectangle shows the location of the NCP. This
216 figure has been repeated for a longer average period, i.e. 1979-2019 (not shown) and the result
217 is similar.

218 2. Data & Methods

219 2.1 Observations, Reanalysis Outputs and PPE Model Simulations

220 Hourly PM_{2.5} concentrations are used from the US embassy site for Beijing for DJF
221 from 2009-2017. Daily mean PM_{2.5} concentrations are constructed using hourly data to

222 evaluate the performance of the HWI as a representative of haze conducive and clear weather
223 conditions for Beijing (see Section 3). We also used newly released gridded daily PM_{2.5}
224 concentrations for DJF from Chinese Air Quality Reanalysis Datasets (CAQRA) provided by
225 China National Environment Monitoring Centre for 2013-2017 (Kong et al., 2021) to test the
226 performance of the HWI across entire China. The CAQRA data has been produced by
227 assimilating surface air quality observations from over 1000 monitoring sites in China and is
228 available at a high spatial resolution of around 15×15 km and hourly temporal resolution over
229 China. More details on the validation of the CAQRA dataset against the independent station
230 data is provided in Kong et al. (2021). The visibility data for Beijing (homogenized data for 20
231 stations in Beijing) is provided by the National Meteorological Information Center of China,
232 China Meteorological Administration (CMA), for DJF 1999-2018.

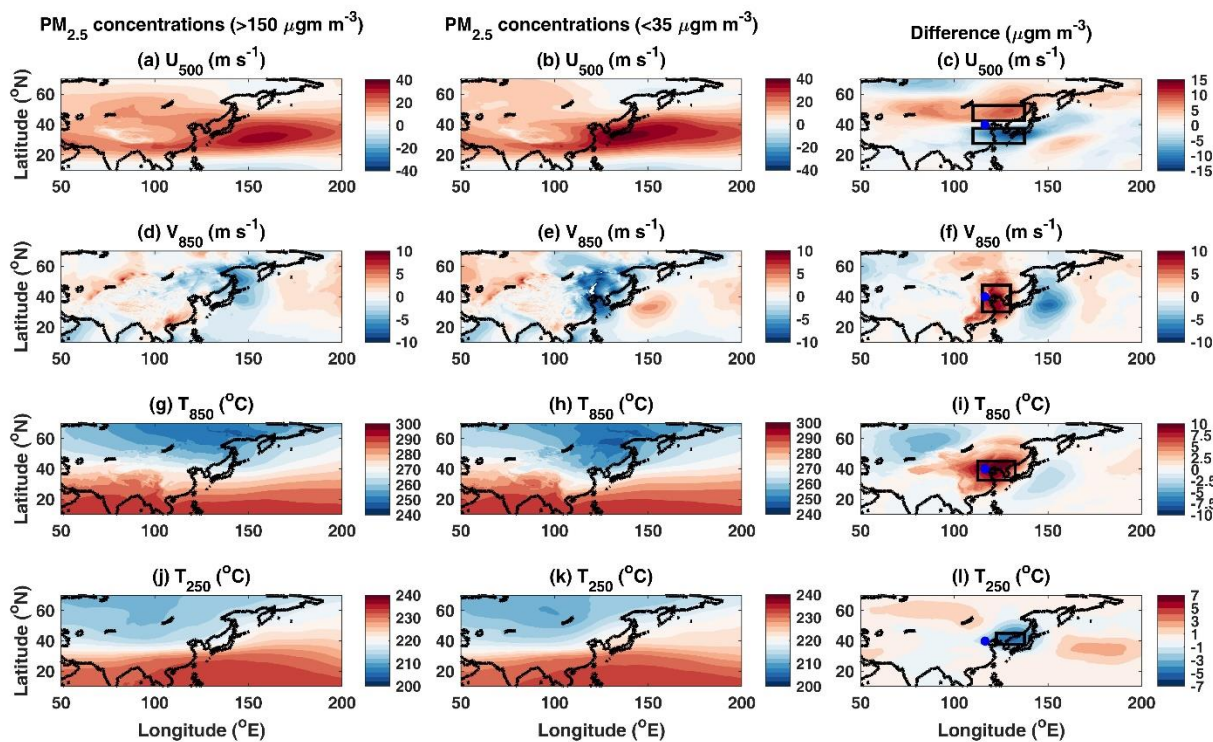
233 We used daily ERA-5 reanalysis data of four variables: meridional wind at 850 hPa
234 pressure level (V_{850}), zonal wind at 500 hPa pressure level (U_{500}), temperatures at 850 hPa
235 level (T_{850}) and 250 hPa (T_{250}) to calculate the HWI for DJF 1979-2019. The ERA-5 data used
236 here is available at 0.25° x 0.25° horizontal resolution and hourly temporal resolution
237 (Hersbach et al., 2020).

238 We used a PPE of climate simulations produced using the recent configuration of the
239 UK Met Office's HadGEM3-GC3.05 coupled model (Sexton et al., 2021; Yamazaki et al.,
240 2021). The base model used for PPE, HadGEM3-GC3.05, has a horizontal resolution of ~60
241 km with 85 vertical levels. A total of 47 model parameters from seven parameterization
242 schemes were simultaneously perturbed to obtain the PPE (the full list of perturbed parameters
243 is provided in Table 1 of (Sexton et al., 2021). Here, we used daily outputs of V_{850} , U_{500} , T_{850}
244 and T_{250} for DJF for the historical (1969-2005) and future (2006-2089) under the RCP8.5
245 scenario. In addition, we also assessed internal variability using 200-year control simulations

246 for each PPE member where 1900 boundary conditions were prescribed. Overall, 16 PPE
 247 members are available for all the control, historical and RCP8.5 simulations

248 2.2 Calculation of the HWI

249 The winter HWI is calculated using the methodology given by Cai et al. (2017). We
 250 analyse the composite differences in the U_{500} , V_{850} , T_{850} and T_{250} for hazy ($PM_{2.5}$ concentrations
 251 $> 150 \mu\text{g m}^{-3}$ for Beijing) and clear ($PM_{2.5}$ concentrations $< 35 \mu\text{g m}^{-3}$ for Beijing) days across
 252 China for DJF 2009-2017 (Fig. 2) (see section 3.1 for an explanation on the $PM_{2.5}$ concentration
 253 cut-offs values used here). We also provide the composite values for these meteorological
 254 variables for hazy and clear days separately in Fig. 2.



255
 256 **Figure 2** Winter composites of u-wind at 500 hPa level (U_{500}) over China for all available days
 257 for which data is available from US embassy station for Beijing for DJF 2009-2017 for (a) high
 258 $PM_{2.5}$ ($>150 \mu\text{g m}^{-3}$), (b) low $PM_{2.5}$ ($<35 \mu\text{g m}^{-3}$) concentrations and (c) difference between
 259 the composites in (a) and (b). (d-f) same as (a-c) but for v-wind at 850 hPa level (V_{850}), (g-i)
 260 same as (a-c) but for temperature at 850 hPa level (T_{850}), and (j-l) same as (a-c) but for
 261 temperature at 250 hPa pressure level (T_{250}). Black rectangles (B1-B5) in the last column show
 262 the regions for which spatial means were used for the calculation of the HWI. The blue dot in
 263 these columns shows the location of Beijing.

264 During the hazy days, the mid-tropospheric westerly flow becomes weaker over the
265 NCP as compared to the clear days (Fig. 2a-c). The mid-tropospheric trough also moves
266 northwards as suggested by the dipole pattern in Fig 2c, which shows the differences in the
267 U_{500} for hazy and clear days. The northerly flow ~~near the surface~~in the lower troposphere is
268 weaker during hazy days as compared to clear days (Fig. 2d-f). The lower troposphere is
269 relatively warmer during hazy days as compared to clear days (Fig. 2g-i) whereas the upper
270 troposphere is cooler over the NCP (Fig. 2j-l). The changes in these variables are also consistent
271 with the previous studies (e.g. Cai et al., 2017) that showed similar changes for this time period.
272 Therefore, we use these four variables for the calculation of the HWI, which is used as a proxy
273 for haze conducive and clear weather conditions under a future climate.

274 For the calculation of observational HWI, we use ERA-5 reanalysis data for the period
275 1979-2019. We first create a daily DJF time series of each variable for each reanalyses grid
276 point over China. The daily DJF time series is concatenated for the period 1979-2019. A daily
277 standardised anomaly time series is created for each meteorological variable by first removing
278 the daily mean climatology from each day of the time series and then normalising by the
279 standard deviation. Spatial averages are then obtained over the relevant boxes (B1 to B5) for
280 each meteorological variable following Cai et al. (2017) (Fig. 1). The HWI time-series is
281 calculated by using the following equation:

$$282 \quad \text{HWI}(t) = U_{500}(t) + V_{850}(t) + dT(t)$$

283 where $U_{500} = U_{500,B1}(t) - U_{500,B2}(t)$, $V_{850} = V_{850,B3}(t)$, and $dT = T_{850,B4}(t) - T_{250,B5}(t)$. The HWI
284 (t) time series is then itself normalized by its own standard deviation.

285 For the PPE historical and RCP8.5 simulations, the daily HWI time series is calculated
286 for each ensemble member for DJF for 1969-2089 using the same methodology as used for
287 ERA-5, with the difference being that the normalisation of the PPE time-series (1969-2089) is

288 performed using the historical standard deviation (1969-2005), following Cai et al. (2017).
289 Similarly, the HWI time series is calculated for the PPE pre-industrial control simulations for
290 170 model years out of 200 model years (the first 30 years are discarded as model spin-up
291 period). The normalisation of the pre-industrial control time series is performed using the
292 standard deviation for 170 years. The pre-industrial control simulations used here are initialised
293 with past forcings corresponding to the year 1900 and therefore are an approximate
294 representation of the internal variability of the current climate as this does not take into account
295 any temporal changes in the internal variability from 1900 to the historical and future periods
296 used here.

297 **3. Haze Weather Index as an indicator for clear and haze conducive weather conditions** 298 **over the NCP**

299 As the HWI was originally proposed for Beijing by Cai et al. (2018), we first determine
300 if the HWI can be used as a representative of haze conducive and clear weather conditions for
301 the present climate for Beijing using (a) $PM_{2.5}$ concentrations from the US embassy station in
302 Beijing and (b) $PM_{2.5}$ concentrations averaged over larger Beijing domain from CAQRA
303 reanalysis and (c) visibility data from the CMA stations in Beijing. We then determine the
304 spatial extent of the region for which HWI can be used as an indicator of haze conducive and
305 clear weather conditions using $PM_{2.5}$ concentrations for China using CAQRA reanalysis data.
306 We use the 25th and 75th percentile values of daily mean $PM_{2.5}$ concentrations to identify the
307 clear and hazy days, respectively for each dataset. For visibility, we use the opposite criterion,
308 i.e. 25th percentile as a threshold for hazy days and 75th percentile as a threshold of clear days,
309 as lower visibility is associated with hazy days and higher visibility with clear days. The days
310 with daily $PM_{2.5}$ concentration or visibility lying between the 25th and 75th percentile values
311 are identified as moderately polluted days.

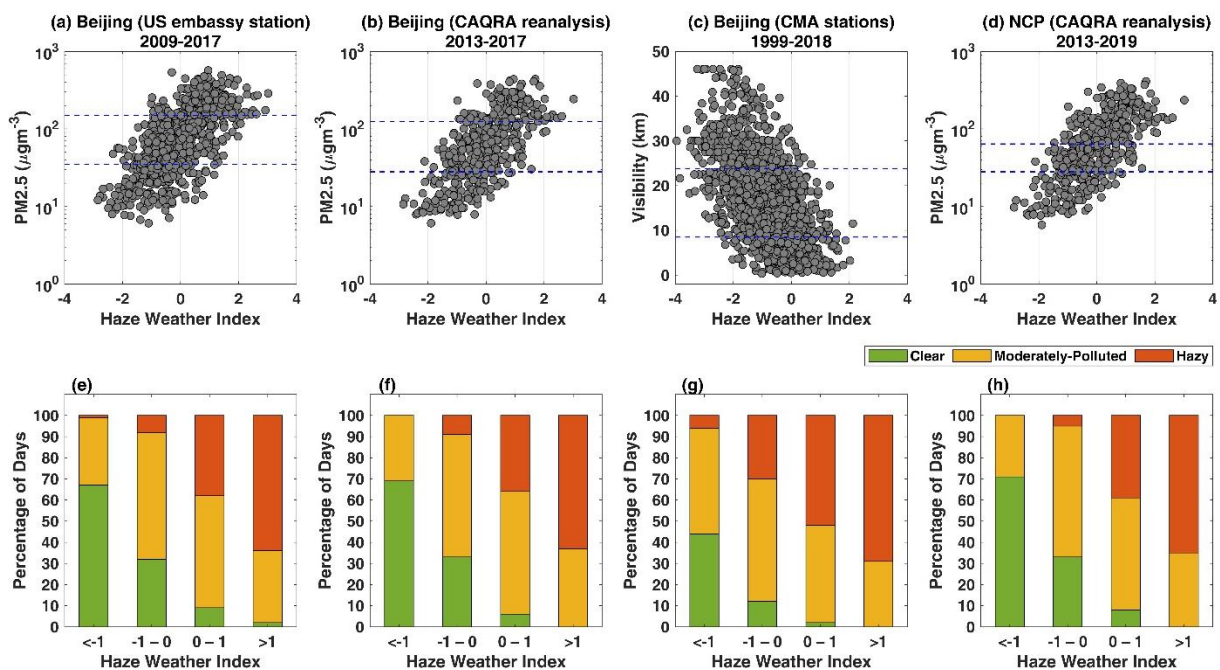
312 3.1 PM_{2.5} concentrations for Beijing versus HWI

313 We examine the relationship between the daily HWI and PM_{2.5} concentrations for the
314 US embassy station for Beijing. Figure 3 (a) shows that the daily HWI increases linearly with
315 increasing PM_{2.5} concentrations for up to $\sim 150 \mu\text{g m}^{-3}$ and $\text{PM}_{2.5} > 150 \mu\text{g m}^{-3}$, the HWI starts
316 to level-off (note the log scaling in the y-axis). The time-series correlation between the HWI
317 and PM_{2.5} concentration is ~ 0.58 , which is significant at the 1% level. Callahan et al. (2019)
318 have also obtained a correlation coefficient of 0.58 for daily PM_{2.5} concentrations from the U.S.
319 embassy in Beijing and the HWI calculated using NCAR R1 reanalysis.

320 The 25th and 75th percentile values of daily mean PM_{2.5} concentrations for the US
321 embassy Beijing station for DJF 2009-2017 are ~ 35 and $\sim 150 \mu\text{g m}^{-3}$ respectively. We
322 determine the percentage of hazy days (with daily mean PM_{2.5} concentrations $> 150 \mu\text{g m}^{-3}$) and
323 clear days (with daily mean PM_{2.5} concentrations $< 35 \mu\text{g m}^{-3}$) for different HWI ranges (Fig.
324 3e). Out of all days with $\text{HWI} > 1$, 64% have daily mean PM_{2.5} concentrations $> 150 \mu\text{g m}^{-3}$ and
325 98% with PM_{2.5} concentrations $> 35 \mu\text{g m}^{-3}$. This suggests that for $\text{HWI} > 1$, almost all days are
326 hazy or moderately polluted. Similarly, almost all days with $\text{HWI} < -1$ are clear or moderately
327 polluted. Using HWI thresholds of ± 1 demarcates between the clear and hazy days, i.e. almost
328 no clear days occur for $\text{HWI} > 1$ and almost no hazy days occur for $\text{HWI} < -1$.

329 We have also examined the relationship between the individual variables in the HWI
330 (section 2.2) and PM_{2.5} concentrations observed at the US embassy in Beijing/CAQRA and
331 find that the individual components have correlation values that are similar to or less than that
332 of those used in the combined HWI. Also, physically multiple favourable weather conditions,
333 as represented by each of these variables, collectively provide a conducive setting for haze.
334 Hence, we focus on the HWI as a combined index rather than its individual components.

335 To examine if the PM_{2.5} concentrations from the US embassy station are sensitive to
 336 the abrupt changes in the local meteorology, e.g. wind speeds or direction, we also examine
 337 the relationship between the HWI and PM_{2.5} concentrations averaged over the domain centred
 338 around Beijing (116.15 – 116.65 °E, 39.65 – 40.15 °N) from the CAQRA reanalysis data (Fig.
 339 3b and 3f). The PM_{2.5} concentrations for region spatially averaged around Beijing from
 340 CAQRA data are in the range 6 μg m⁻³ – 441 μg m⁻³ and from the Beijing US embassy station
 341 are 6 μg m⁻³ – 569 μg m⁻³ suggesting the values from both data sources are comparable. The
 342 correlation coefficient is ~0.58, which is the same as the correlation obtained using the US
 343 embassy data. The total number of hazy, clear and moderately polluted days for different HWI
 344 ranges also show similar results for both datasets (Fig. 3e-3f). This implies that the HWI
 345 relationship with PM_{2.5} concentrations is robust across different data sources and that PM_{2.5} is
 346 a regional pollutant.



347 **Figure 3** HWI versus daily mean (a) PM_{2.5} concentrations for the US embassy Beijing station for DJF
 348 2009-2017 (b) PM_{2.5} concentrations spatially averaged over the region around Beijing (116.15-116.65
 349 °E, 39.65 - 40.15 °N) from CAQRA reanalysis for DJF 2013-2017 (c) visibility averaged over 20
 350 stations from the CMA for DJF 1999-2018 and (d) PM_{2.5} concentrations spatially averaged over the
 351 NCP (36-43.5 °N, 107-122 °E) from CAQRA reanalysis. Blue lines show the 25th and 75th percentile
 352 thresholds used to define clear and hazy days for each dataset. Percentage of clear, moderately polluted
 353 and hazy days for different HWI ranges for the (e) US embassy Beijing station for DJF 1999-2018 (f)
 354 US embassy Beijing station for DJF 2009-2017 (g) Beijing (CMA stations) for DJF 1999-2018 (h) NCP (CAQRA reanalysis) for DJF 2013-2019.

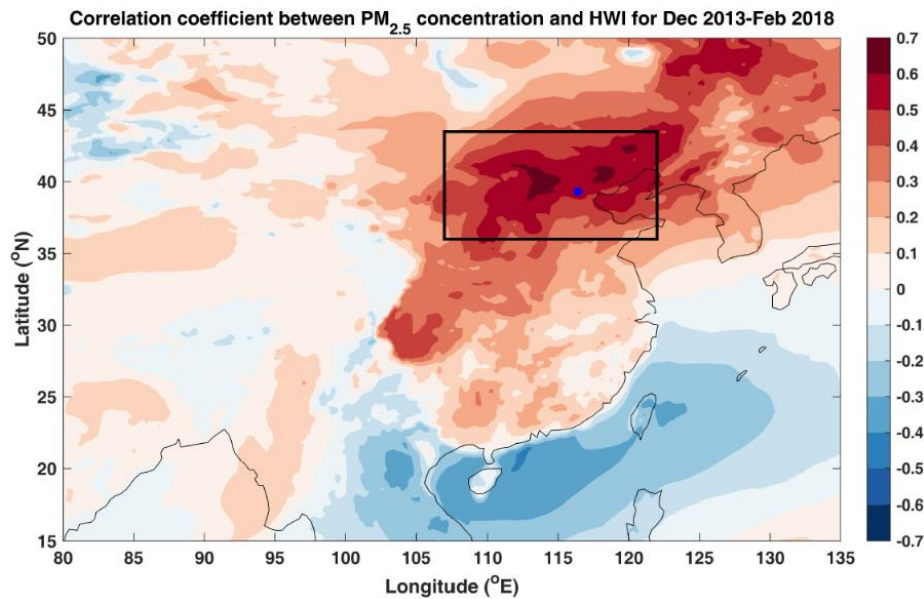
355 larger Beijing domain (116.15-116.65 °E, 39.65 - 40.15 °N) from CAQRA reanalysis for DJF 2013-
356 2017 (g) Beijing for DJF 1999-2018 (h) NCP from the CAQRA reanalysis for DJF 2013-2017.

357 **3.2 Visibility for Beijing versus HWI**

358 As visibility is an optical representative of haze (Wang et al., 2006) and the data for
359 visibility is available for a relatively long period (1999-2018) as compared to the PM_{2.5}
360 concentrations, we also correlate the HWI with the visibility over Beijing. Figure 3 (c) shows
361 that the HWI is inversely related to the visibility for the Beijing station. The time-series
362 correlation between the HWI and visibility is -0.63, which is significant at the 1% level. The
363 days with visibility < 8.5 km are identified as hazy days, days with visibility > 23.8 km are
364 identified as clear days. For days with HWI > 1, no clear days occur and similarly for days with
365 HWI < -1, only 6% of days are hazy (Fig 3g). This further confirms that the correlation between
366 the HWI and haze is significant for a longer period (1999-2018) using visibility as a metric for
367 haze (alternative to the PM_{2.5} concentrations used above).

368 **3.3 PM_{2.5} concentrations over North China Plain versus HWI**

369 We now determine the spatial extent for which HWI can be used as an indicator of haze
370 clear or haze conducive conditions using PM_{2.5} concentrations from CAQRA reanalysis. We
371 correlate the daily time-series of PM_{2.5} concentration at each grid point with the HWI for DJF
372 2013-2017 (Fig. 4). Over the entire NCP (36-43.5 °N, 107-122 °E), the correlation coefficient
373 between the daily HWI and gridded PM_{2.5} concentration is ~0.7, significant at the 1% level.
374 The correlation is considerably lower but still significant over other eastern China regions, e.g.
375 north easternmost China and the Sichuan Basin (27-32 °N, 102-107 °E).



376

377 **Figure 4** Spatial distribution of correlation between winter PM_{2.5} concentrations and HWI time series
 378 at each grid point. Blue dot shows the Beijing station (39.3 °N, 116.4 °E) and the black rectangle shows
 379 the North China Plain (36-43.5 °N, 107-122 °E).

380

Considering daily mean PM_{2.5} concentrations averaged over the NCP, we also find a
 381 linear relationship with the daily HWI ($r = 0.66$; significant at the 1% level; Fig 2d). We also
 382 calculate the percentage of clear and hazy days for different HWI ranges for the larger domain
 383 of the NCP using the 25th and 75th percentile values, respectively. The percentage of hazy and
 384 clear days for HWI > 1 and HWI < -1 for NCP in CAQRA reanalyses are very similar to the
 385 values obtained for the US embassy Beijing station (Fig 3h).

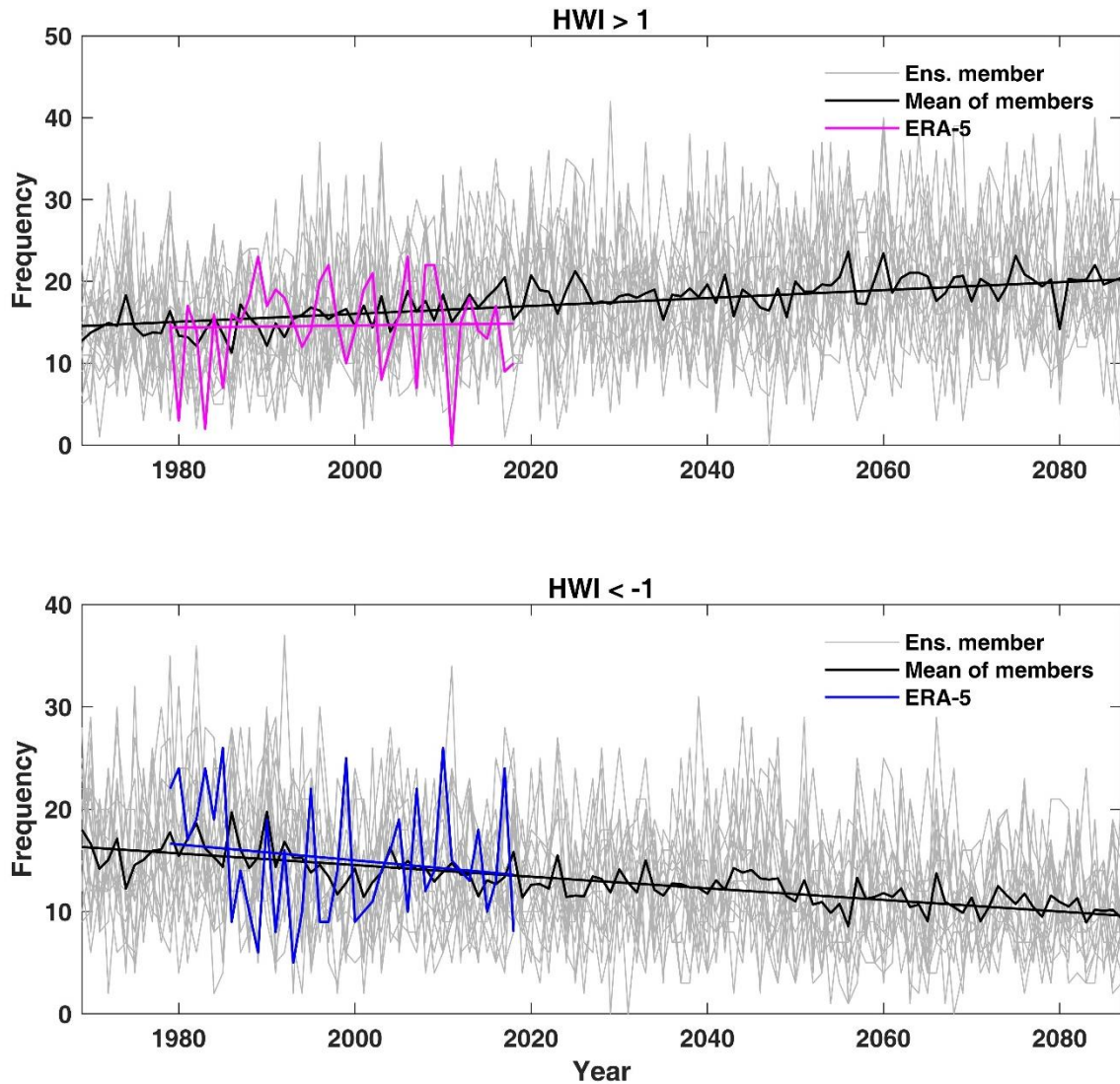
386

Overall, our results confirm that the daily HWI has a robust relationship with daily
 387 PM_{2.5} concentrations not only for the Beijing station but across the NCP for the given time
 388 periods. Therefore, we use HWI > 1 as a proxy for haze conducive weather and HWI < -1 as a
 389 proxy for clear weather across the NCP region. This threshold is also consistent with several
 390 other studies (e.g., Cai et al., 2017; Callahan and Mankin, 2020; Callahan et al., 2019), that
 391 have used HWI >1, as a cut-off for haze conducive weather for Beijing. We now calculate the
 392 frequency of haze conducive weather (HWI >1) and clear weather (HWI < -1) for the past and
 393 future using ERA-5 reanalysis and PPE members.

394 **4. Historical and future changes in haze conducive and clear weather occurrence**

395 The frequency of haze conducive weather ($HWI > 1$) and clear weather ($HWI < -1$) from
396 the ERA-5 reanalyses and the PPE are shown in Fig. 5. For ERA-5, the frequency of haze
397 conducive weather has increased, whereas the frequency of clear weather ($HWI < -1$) has
398 reduced for the period 1979-2018. The mean frequency of haze conducive weather using 16
399 PPE members shows a relatively larger increase than ERA-5 for the same 1979-2018 time
400 period (Fig. 5a). In contrast, the mean frequency of clear weather from the PPE for this period
401 shows a similar reduction to that obtained using the ERA-5 reanalyses (Fig. 5b).

402 We examine the changes in the frequency of haze conducive weather ($HWI > 1$) and
403 clear weather ($HWI < -1$) for the historical (1979-2005) and three future periods, i.e. near (2006-
404 2032), mid (2033-2059) and far (2060-2086) future. The mean frequency for haze conducive
405 weather is 14.7 days per winter obtained from the ERA-5 reanalysis and 15.0 days per winter
406 from the PPE mean for the historical period. The corresponding values for clear weather are
407 15.0 days and 15.2 days per winter for ERA-5 and PPE, respectively. This shows a good
408 agreement between the mean frequencies of haze conducive and clear for the ERA-5 data and
409 the PPE mean for the historical period.

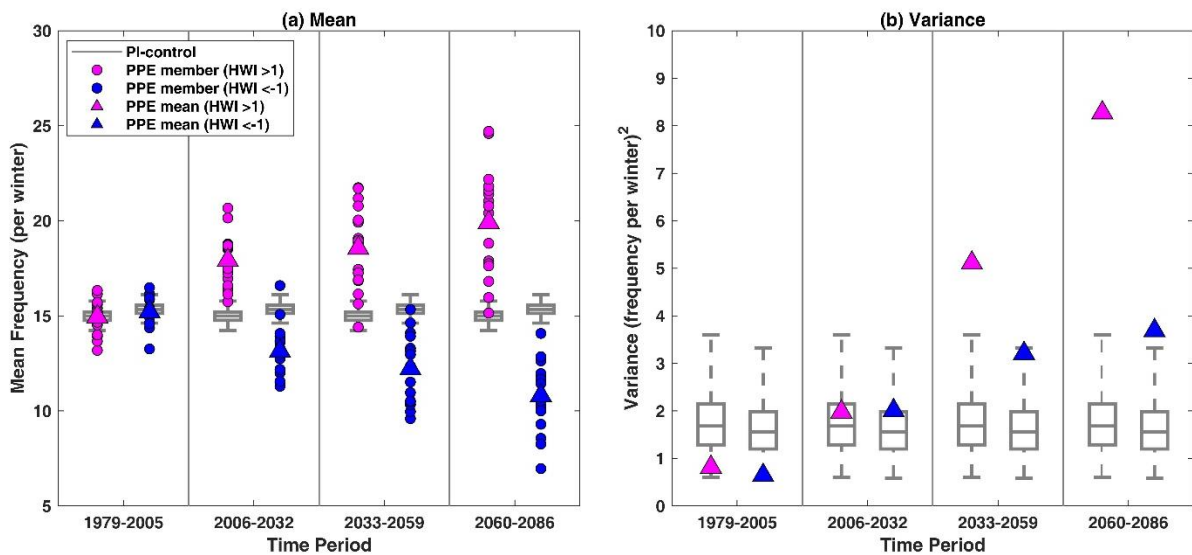


410

411 **Figure 5** Frequency of haze conducive weather (HWI>1, pink line) and clear weather (HWI<-1, blue
 412 line) per winter from ERA-5 reanalysis (1979 to 2018). Year 1979 represents period from 1 December
 413 1979 to 28 February 1980 and so on. For each winter (DJF), we calculate the total number of days with
 414 HWI>1 as proxy for haze conducive weather and HWI < -1 as proxy for clear weather conditions. Grey
 415 lines show frequencies from 16 individual PPE members and black line shows the mean of frequency
 416 using all 16 PPE members for 1969-2087 under the RCP8.5 scenario. Linear trend is calculated using
 417 the line of best fit.

418 The mean frequency of haze conducive weather for near, mid and far future is 17.9,
 419 18.6 and 19.9, respectively. The mean frequency for the same future periods for clear weather
 420 is 13.2, 12.2 and 10.8, respectively (Fig. 6a). The mean change in the frequency of haze
 421 conducive weather averaged across all PPE members is 20%, 24% and 33% for the near, mid
 422 and far future respectively as compared to the historical period, suggesting that the frequency
 423 of haze conducive weather will likely increase for all future periods (Fig. 6a). However, there

424 exists a very large range in the projected change for all three future periods suggesting internal
 425 variability or parametric effect could influence the future projections of haze conducive
 426 weather. For the near and mid future, days with $HWI > 1$ are projected to change by -1% to 41%
 427 and -12% to 65% across the 16 PPE members, respectively, as compared to the frequency for
 428 the historical period. For the far future, the range of projected change is even larger, and an
 429 increase of $\sim 87\%$ in the frequency of haze conducive weather is also possible. It is noted that,
 430 for all three periods, only one of the sixteen ensemble members (E16 shown in Fig. 10) shows
 431 a reduction in the haze conducive weather frequency whereas other ensemble members show
 432 an increase in frequency for all periods. For the historical period, E16 ensemble member has a
 433 mean frequency of 16.3, which reduces to 16.2, 14.4 and 15.2 for near, mid and far future.
 434 While E16 ensemble member shows a consistent reduction in mean frequency in future, the
 435 reduction is specific to only this ensemble member and is not a general feature across PPE
 436 members.



437

438 **Figure 6** (a) Mean frequency of haze conducive weather ($HWI > 1$, pink) and clear weather ($HWI < -1$,
 439 blue) for the historical period (1979-2005), near (2006-2032), mid (2033-2059) and far (2060-2086)
 440 future under the RCP8.5 scenario. Circles represent PPE members and triangles PPE mean. Grey box
 441 and whiskers show the distribution of 10,000 values of mean frequencies sub-sampled from the control
 442 simulation, (b) same as (a) but shows variance across 16 PPE members for each period. For box and
 443 whiskers, we first randomly sampled 10,000 time series of length 27 years using 2704 years of pre-
 444 industrial control simulation and calculated 10,000 values of mean frequency. We then randomly sub-

445 sample 16 mean values (corresponding to the number of ensemble members) from the 10,000 mean
446 values, calculated their mean for (a) and variance for (b). This is repeated 10,000 to obtain a distribution.
447 The boxes are at the 25th and 75th percentile and the whiskers at 2.5th and 97.5th percentile of mean and
448 variance distribution. For panel (a), the box and whiskers are comparable only to the ensemble means
449 (triangles) and not ensemble members (circles).

450 For clear weather ($HWI < -1$), the mean change in the frequency averaging across all
451 PPE members is -13%, -20% and -29% for near, mid and far future, respectively (Fig 6a).
452 Considering the range across the 16 PPE members, the frequency of clear weather for near,
453 mid and far future is projected to change by -29% to 25%, -36% to 10% and -57% to -9%,
454 respectively. Overall, most ensemble members show an increase in the frequency of haze
455 conducive weather and a reduction in the frequency of clear weather for all three future periods.
456 However, negligible change or even the opposite change, though less likely, but possible for
457 all periods.

458 We also determine the influence of anthropogenic climate change and the parametric
459 effect on the frequencies of haze conducive weather ($HWI > 1$) and clear weather ($HWI < -1$) for
460 the historical as well as the three future periods. As shown in later Section 5, the estimate of
461 interannual variance from the control is representative of all time periods and shows no
462 discernible parametric effect. Therefore, we pool the 16 PPE control simulations to sample the
463 internal variability for box and whiskers shown in Fig. 6 (a) and 6 (b) (see captions for details
464 on resampling).

465 In Fig. 6 (a), we show the mean frequency of haze conducive weather and clear weather
466 for 16 individual PPE members (circles) and PPE mean (triangles). The grey box and whiskers
467 represent the range of ensemble mean frequencies that can be explained by the internal
468 variability. If the PPE mean (triangles) lies within the whiskers (i.e. 95 percentile of the control
469 distribution) we conclude no influence of anthropogenic climate change on mean frequency
470 however if the PPE mean lies outside the whiskers, it would represent a climate change signal
471 in the mean frequency. Figure 6 (a) suggest that the mean frequencies for haze conducive as

472 well as clear weather lies within the box-whiskers for the historical but lies outside the whiskers
473 for the three future periods, thereby showing a clear impact of anthropogenic climate change
474 on the frequencies of both haze conducive and clear weather conditions.

475 We now examine whether the differences in the mean frequency across different PPE
476 members (shown by circles in Fig. 6a) for a given period can be explained by the internal
477 variability or if the differences in PPE members partly arise due to the parametric effect. The
478 triangles in Fig. 6b shows the variance across 16 PPE members, i.e. variance across 16 circles
479 shown in Fig. 6a, for each time period. The whiskers in Fig. 6b show the 95th confidence
480 interval from the control simulation and is representative of the internal variability. For any
481 time period, if the PPE member variance (triangle) lies within the whiskers, we conclude that
482 the differences in mean frequencies in Fig. 6a can be fully explained by the internal variability
483 and there is no discernible impact of the parametric effect. However, if the triangles lie outside
484 the whiskers in Fig. 6b, we conclude an impact of the parametric effect on the mean frequency
485 for that period. For the points that lie outside the whiskers in Fig. 6b, we also quantify the
486 percentage of variance that can be explained by the internal variability and parametric effect.
487 For any time period, the variance in ensemble mean due to the parametric effect is simply
488 calculated as follow and the remaining variance is attributed to the internal variability.

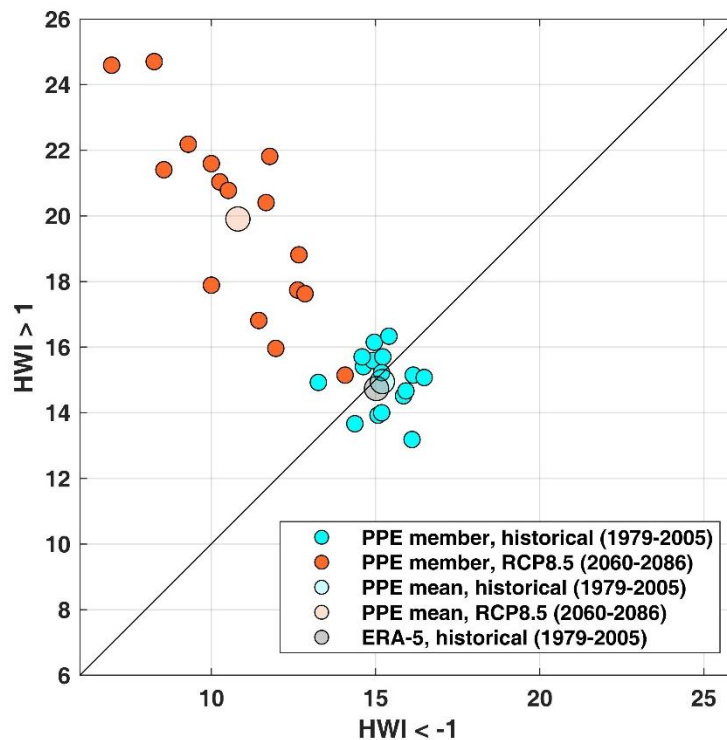
$$489 \quad \frac{\text{Total variance in the ensemble mean} - \text{Mean variance from the control simulation}}{\text{Total variance in the ensemble mean}} \times 100$$

490 Figure 6b shows that the difference variance in PPE mean frequency-frequencies across
491 PPE members (as shown by PPE member variance) is small for the historical and near future
492 but increases for mid and far future periods. For the historical and near future periods, the PPE
493 member variance lies within the range sampled by the internal variability for both haze
494 conducive weather (HWI>1) and clear weather (HWI<-1). This shows that there is no

509 discernible influence of the parametric effect on the frequency of haze conducive weather or
510 clear weather conditions for the historical and near future periods.

511 For mid-future, the PPE member variance for clear weather lies within the whiskers
512 and therefore no discernible influence of the parametric effect is detected. In contrast, the PPE
513 member variance for -in-haze conducive weather lies outside the whiskers and whereas the
514 variance for clear weather lies within the whiskers. For mid future and for haze conducive
515 weather, and the internal variability can explain ~33% of the variance across PPE members
516 and the remaining ~67% arises due to the parametric effect.

517 -For the far future, triangles corresponding to both haze conducive and clear weather
518 lies well outside the whiskers and therefore show a clear influence of parametric effect. Only
519 ~20% of the variance in the frequency of haze conducive weather and ~43% variance in the
520 frequency of clear weather can be explained by the internal variability and the remaining 80%
521 and 57% respective variance in the frequencies arise due to the parametric effect.



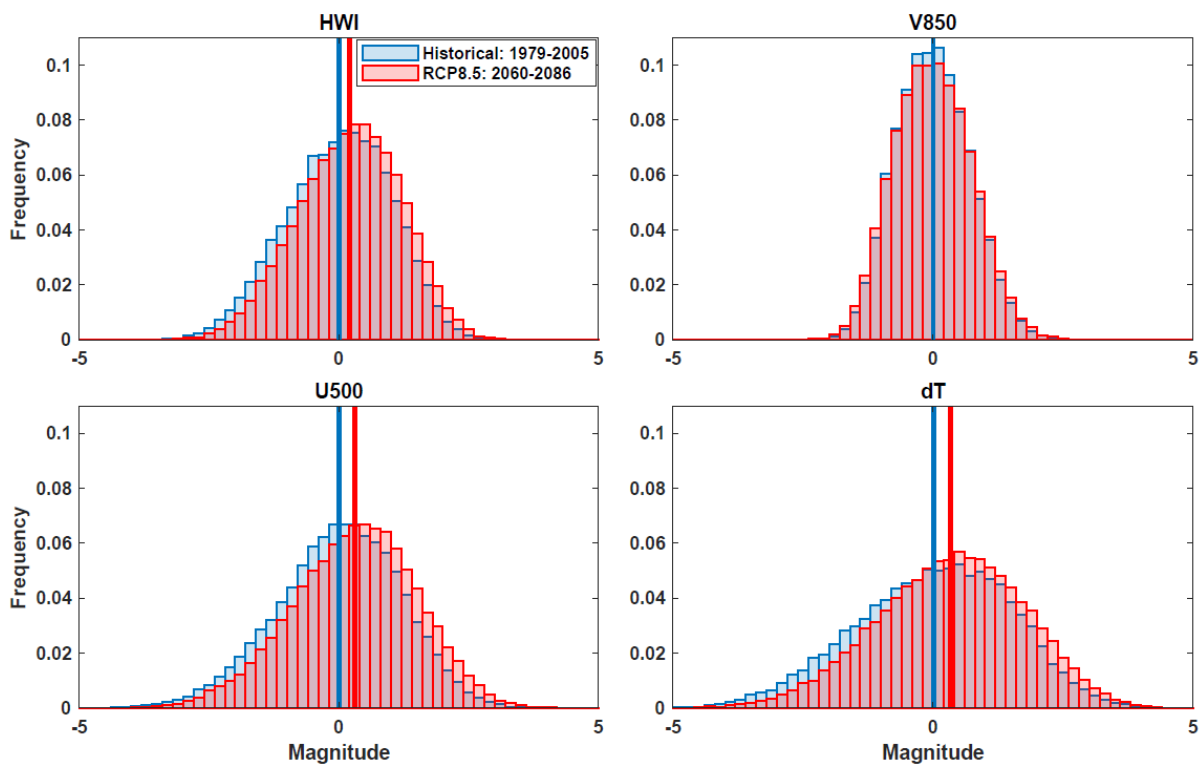
522

523 **Figure 7** Frequency of haze conducive weather ($HWI > 1$) versus clear weather ($HWI < -1$) averaged over
524 the historical period (1979-2005) and the far-future (2060-2086) period under RCP8.5 using all PPE
525 members. Circles denote individual PPE members whereas triangles denote the mean of the members.
526 Grey triangle shows mean frequency from ERA-5 reanalysis for the historical period (1979-2005). The
527 black solid line shows the 1:1 (identity) line.

528 In addition to the changes in the frequencies over time, we also investigate the relative
529 changes in the frequency of haze conducive weather ($HWI > 1$) versus clear weather ($HWI < -1$).
530 The average haze conducive and clear weather frequency over the historical period are almost
531 equal for each PPE member (Fig. 7). All PPE members show a higher frequency for haze
532 conducive weather than clear weather under the far future (2060-2085), however, there exists
533 a substantial range in this change. The frequency of winter haze conducive weather can be
534 similar or up to 3.5 times the frequency of clear weather conditions (Fig. 7). Similar results are
535 also obtained for the near and mid-future. Averaged across the PPE members, the number of
536 haze conducive days can increase by ~ 2 times as compared to the number of clear days in
537 future. As noted in Fig. 7, the spread in the haze conducive weather frequency amongst
538 individual ensemble members is also larger for the far future (2060-2086) compared to the
539 historical period. This suggests a larger uncertainty and a larger range of possible future
540 meteorological conditions affecting haze and air quality as compared to the historical period.
541 Other studies have (e.g., Cai et al., 2017; Callahan and Mankin, 2020) also found similar
542 increases in the frequency of haze conducive weather for the future. However, the range of
543 projected change differs substantially across models as well as ensemble members. In our
544 study, in addition to the frequency of haze conducive weather, we also evaluate the changes in
545 the frequency of clear weather across different future periods and compared the relative
546 changes in both the frequencies, which is not examined in the past studies.

547 We now investigate changes in the distribution of the HWI as well as individual
548 constituents of the HWI between the far future (2060-86) and the historical (1979-2005) period.
549 The probability distribution of the HWI shows a shift in the distribution towards higher

550 magnitudes for the far future as compared to the historical period (Fig. 8). This implies an
 551 increased frequency of haze conducive weather, as the number of days with $\text{HWI} > 1$ increase.
 552 A similar shift is apparent in the zonal-mean wind (U_{500}) and the vertical temperature profiles
 553 (dT), whereas no apparent shift is noted in V_{850} . We also find that the shift in the HWI, as well
 554 as U_{500} and dT distribution, is not due to the shift in one particular PPE member or time period.
 555 It is consistent across the 16 PPE members and is continual over time from the historical to the
 556 far-future period. Therefore, for the PPE analysed here, the changes in the haze conducive
 557 weather ($\text{HWI} > 1$) is largely associated with the changes in the U_{500} and dT , and V_{850} appear to
 558 have a less important role. Despite using a multimodel ensemble and a different time period
 559 than used here, a similar result with a relatively larger shift in the PDFs of U_{500} and dT as
 560 compared to V_{850} can also be noted in the Cai et al. (2017).



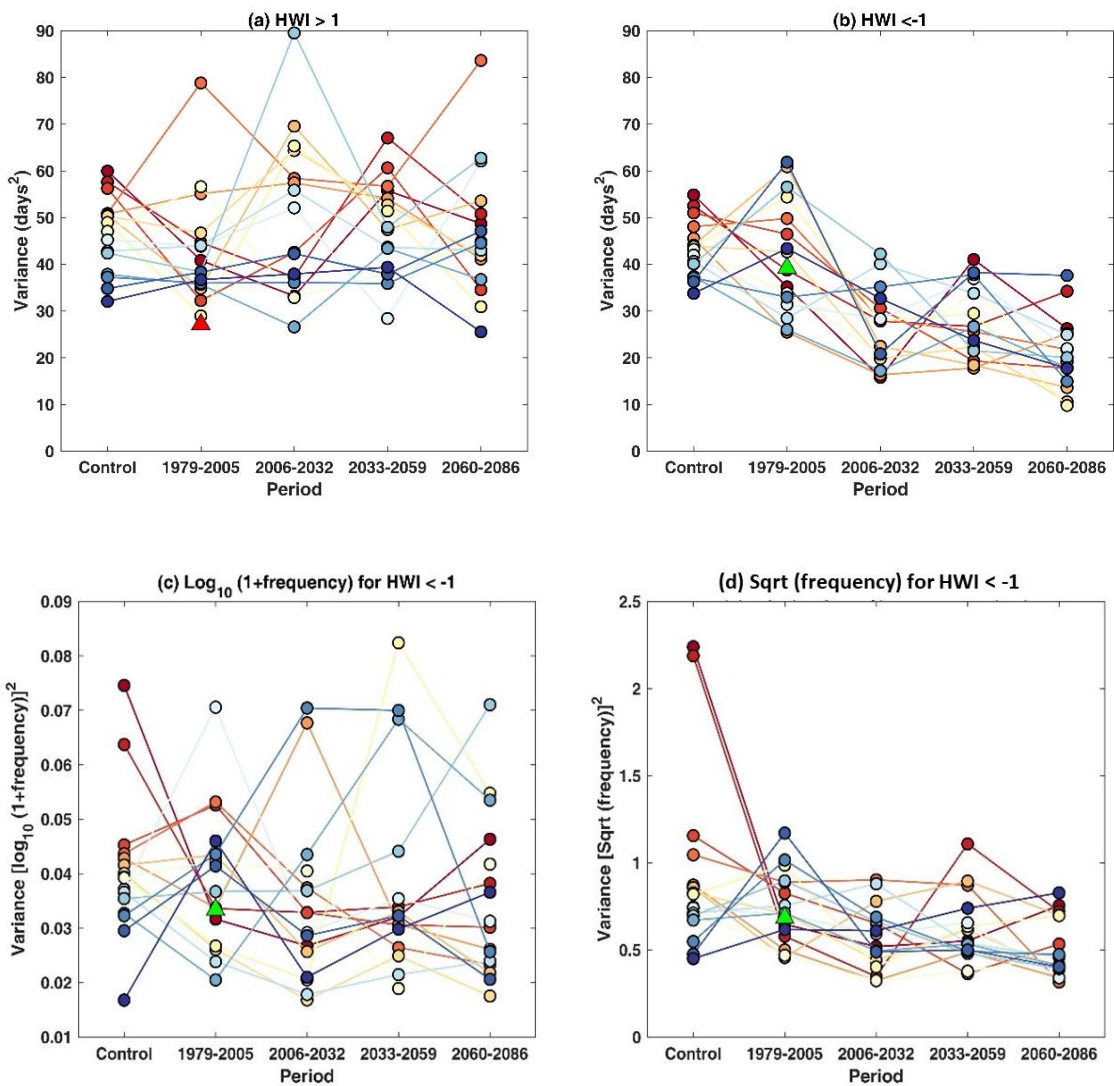
561

562 **Figure 8** Probability Distribution Functions (PDF) for the winter HWI, meridional winds at
 563 850 hPa pressure level (V_{850}), zonal winds at 500 hPa pressure level (U_{500}) and temperature
 564 gradient between the lower and upper troposphere (dT). The PDF for the HWI is created using
 565 the daily DJF time series of all 16 PPE members. PDFs for V_{850} , U_{500} and dT are created using
 566 the normalized daily DJF time series of each variable calculated for the HWI (see section 2.2

567 for details) and represents the constituent variables of the HWI. Blues bars show the PDFs for
 568 the historical period and red for the far future under the RCP 8.5 scenario. Blue and red solid
 569 lines show the mean values of the PDF for historical and far future, respectively.

570 **5. Interannual variability in haze conducive and clear weather frequency**

571 Large interannual variability in the frequency of haze conducive (HWI>1) and clear
 572 weather (HWI<-1) is apparent in both individual PPE members and ERA-5 reanalysis (Section
 573 4). Therefore, we examine the changes in the interannual variance of the frequencies for future
 574 periods as compared to the historical period. We also compare the variance in historical and
 575 future time periods with the variance in the control simulation to discern the influence of the
 576 model physical parameterisations, i.e. parametric effect, on the variance.



577

578

579 **Figure 9** Interannual variance in frequency of winter (a) haze conducive weather (HWI>1) and (b)
580 clear weather (HWI<-1) for the control simulation, historical (1979-2005), and near (2006-2032), mid
581 (2033-2059) and far-future (2060-2086) under RCP8.5 for all 16 PPE members. Coloured circles are
582 for individual PPE members and triangles for ERA-5 reanalysis. (c-d) are same as (b) but with \log_{10}
583 and square root power transformations. For (c-d), we first calculate the \log_{10} of (1+frequency) and
584 square-root of the frequency of clear days for the control simulation and each time-period, and then
585 estimate variance for each respective period. The length of control simulation and all future periods is
586 the same as historical, i.e. 27 years. The 27 years used for control here are randomly selected from 170-
587 year control simulation for each member.

588 The interannual variance for ERA-5 data is 27 days² and 39 days² for haze conducive
589 and clear weather, respectively, for the historical period (1979-2005) (triangles in Fig. 9a-b).
590 The interannual variance in haze conducive weather frequency derived from the PPE members
591 for the historical period is larger than that for the ERA-5, whereas for the clear weather the
592 variance for ERA-5 lies within the range of the PPE members. No consistent change in the
593 interannual variance of haze conducive weather is noted for any of the PPE members (note the
594 changes in colour ranking) from the historical to the future periods suggesting little influence
595 of the parametric effect on the interannual variance of haze conducive weather.

596 In contrast, the frequency of clear weather for most PPE members show a marked
597 reduction in the interannual variance from historical to near-future (Fig. 9b). However, as the
598 frequency of clear weather show a decreasing trend in time (see Fig. 5b), the mean frequency
599 would be expected to reduce for the three future periods. Also, the reduction in variance could
600 arise as the frequencies of clear weather approach their lower bound of zero. With count data,
601 a power transformation is often applied to stabilize the variance across all time periods. We
602 applied two power transformations, i.e. $\log_{10}(1+x)$ and square-root (x), where x is the count
603 data (Fig. 9c-d). We find the spread in the variance in the control simulation across the PPE
604 members is comparable with the historical as well as future periods (Fig. 9c-d). Note that for
605 control simulation we randomly selected 27 years (length same as historical and future periods)
606 from 170 years of control simulation from each PPE member, however, we note comparable
607 variance for the other randomly selected samples. Figure 9 (c-d) also shows that the individual

608 PPE members show inconsistent changes in the variance (noting changes in the colour ranking)
609 from control to historical and future periods. Therefore, no robust changes in the interannual
610 variance of haze conducive and clear weather can be detected from control to historical and
611 future periods. This means we can use the variance in the control simulation as a representative
612 estimate of internal variability. This enables us to quantify the influence of the parametric effect
613 and anthropogenic climate change on the mean frequencies (see previous section) and trends
614 in frequencies (see next section) across different periods.

615 **6. Influence of the anthropogenic climate change and parametric effect on trends**

616 We discern the influence of the anthropogenic climate change and parametric effect on
617 the future projections of the trends in the frequency of haze conducive weather ($HWI > 1$) and
618 clear weather ($HWI < -1$). The time series of the haze conducive and clear weather frequency
619 from ERA-5 and the 16 PPE members for the historical and future periods is shown in Fig. 11
620 (a) and 11 (b). The 95th percentile values (blue shaded region) and the range (blue dotted lines)
621 in the haze conducive and clear weather frequency from the respective control simulation for
622 each PPE member are also shown.

623 For haze conducive weather ($HWI > 1$), the time series for selected PPE members (e.g.
624 E3, E4) show increasing positive trends. In particular, towards the end of the 21st century (Fig.
625 10a), the lower half of the control range is seldom sampled and more than the expected number
626 of values lie above the 97.5th percentile of the control frequencies. In contrast, for other PPE
627 members (e.g. E8, E10), the full time series sample the control distribution evenly throughout
628 the full period. For clear weather ($HWI < -1$), some members (e.g. E3, E4) show a clear
629 reduction during the 21st century whilst others (e.g. E16) show no trend and explore the control
630 distribution evenly (Fig 10b).

631 In Section 4, we examined the influence of anthropogenic climate change and
632 parametric effect on the mean frequencies. The analysis of mean frequencies provides an
633 estimate of the accumulated influence of climate change on frequencies with respect to the
634 control simulations whereas analysis of trends would provide a better estimate of changes
635 within a selected time period. Therefore, we apply the same analysis on the trends in the
636 frequencies (Fig. 11).

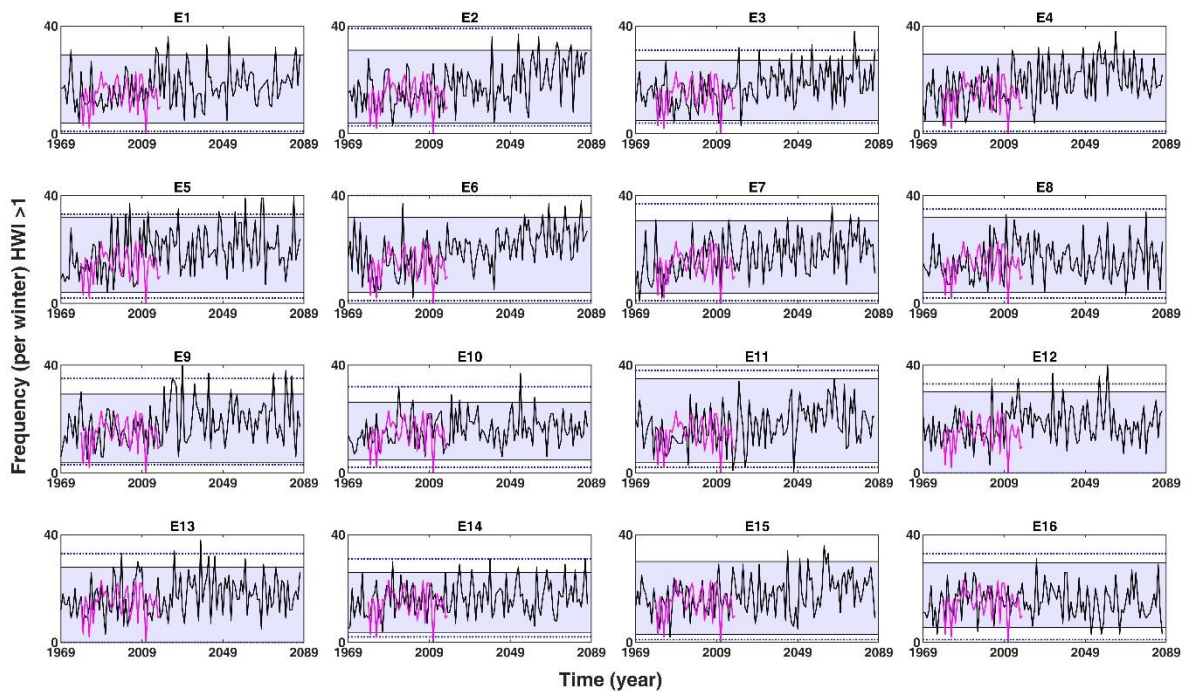
637

638

639

640

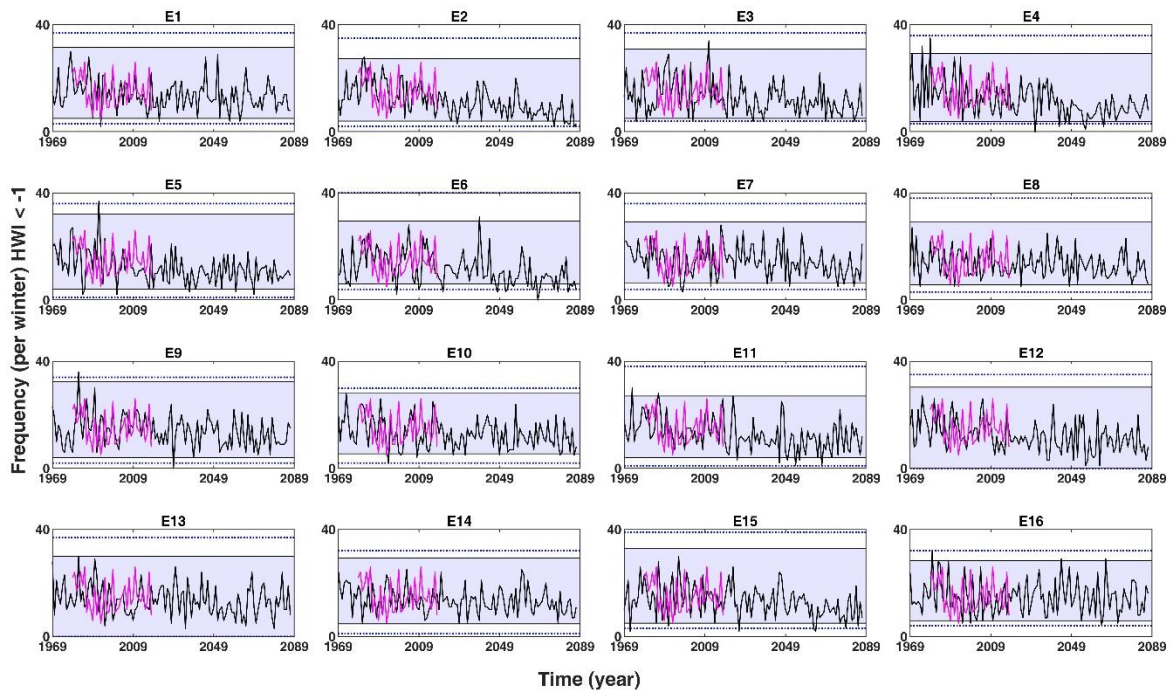
(a) HWI>1



641

642

(b) HWI<-1



643

644 **Figure 10** Frequency of (a) haze conducive weather ($HWI > 1$) and (b) clear weather ($HWI < -1$) per
 645 winter for individual PPE members (black line) under the historical and RCP8.5 scenarios for 1969-
 646 2087 and ERA5 reanalysis (pink line) for 1979-2018. Blue shaded region shows the 95th confidence
 647 interval and blue dashed line shows the range of the frequency of haze conducive and clear weather for
 648 the pre-industrial control simulation of 170-years.

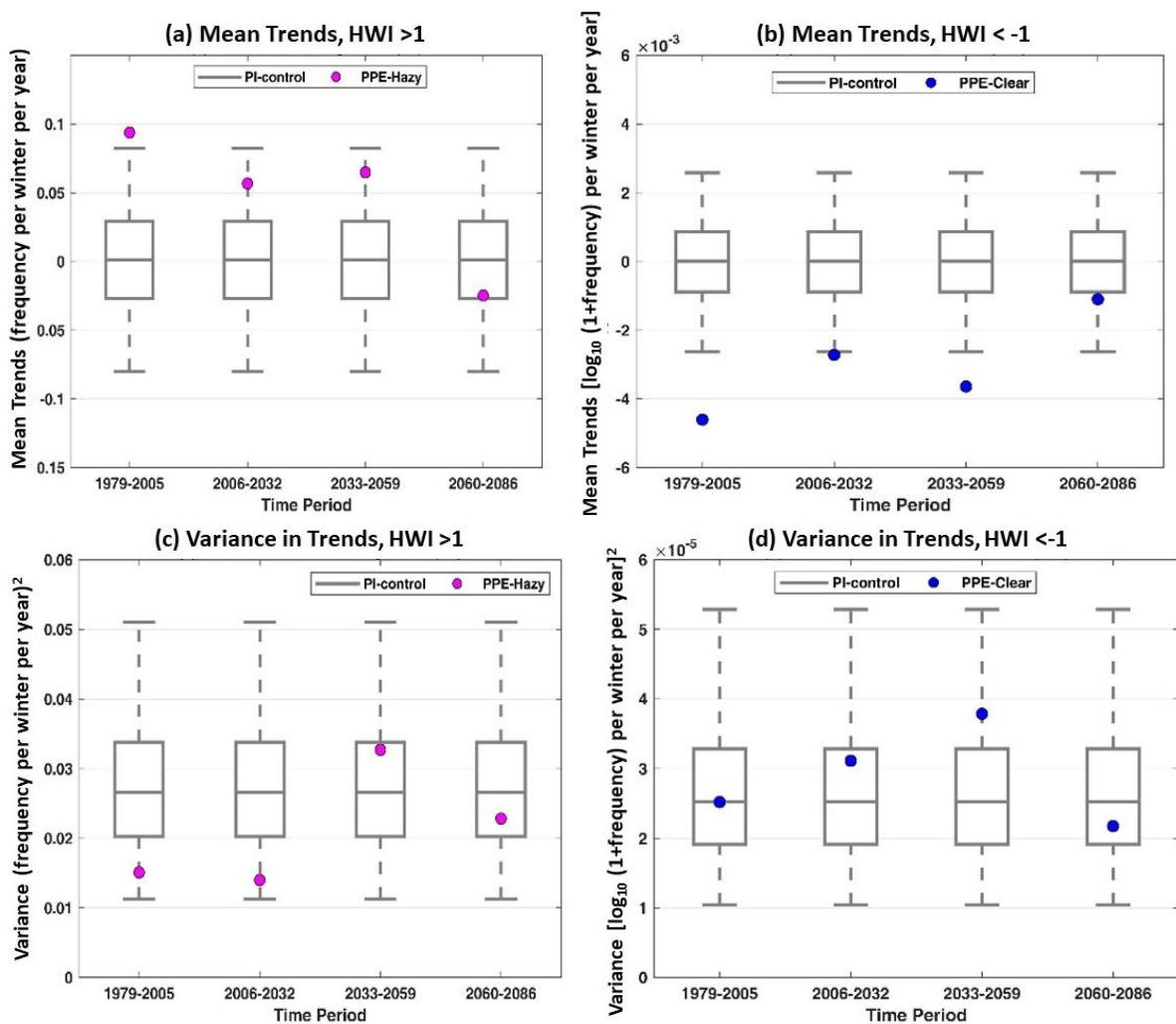
649 We calculate the ensemble mean trend obtained from the 16 individual PPE member
 650 trends to determine the influence of climate change for the historical period (see captions of
 651 Fig. 11 for details). We describe the evolution of the historical trend for three equal-length
 652 future time periods (i.e. near, mid and far future) and examine if the historical trends are
 653 sustained across the 21st century and if the trends are discernible outside the range described
 654 by the internal variability (Fig. 11a-b). The grey whiskers in Fig. 11 (a) and (b) cover the range
 655 of trends that can be explained by internal variability and any trend values lying outside the
 656 grey whiskers represent the influence of anthropogenic climate change.

657 The mean trend in the frequency of both haze conducive ($HWI > 1$) and clear weather
 658 ($HWI < -1$) for the historical period (1979-2005) lie outside the 95% confidence interval of the
 659 control simulations. This suggests that the trends noted for the historical period cannot be
 660 explained by internal variability alone and there is a substantial impact of anthropogenic

661 climate change on the historical trends. The trends in haze conducive weather lie within the
662 envelope of internal variability for the three future periods analysed here implying that the
663 historical trend is not sustained over the 21st century and indistinguishable from the internal
664 variability for the future. Figure 11 (a) also shows a positive mean trend in haze conducive
665 weather ($HWI > 1$) for historical, near and mid future, but a weak negative trend for far future.
666 While the frequency of haze conducive weather increases for all three future periods with
667 respect to the historical period as shown in Fig. 6a, the trends only show an increment or
668 reduction for that period as these are not referenced to the historical period. Therefore, trends
669 could still be negative within any selected period, as in the case of the far future. In contrast,
670 the mean trends in clear weather frequency for near (2006-2032) and mid future (2033-2059)
671 lie outside the 95% confidence interval of the control simulation. This shows that for clear
672 weather frequency ($HWI < -1$), the historical trend is sustained over the first half of the 21st
673 century and then it levels off.

674 We now examine the influence of the parametric effect on the trends in the frequency
675 of haze conducive and clear weather. In Fig. 11 (c) and (d), we show the variance in trends for
676 the time series resampled using the control simulation (see captions for details on resampling).
677 The grey box and whiskers show the 95th confidence interval of the control variance used to
678 represent the internal variability. The variance in PPE trends calculated using 16 PPE members
679 for selected time periods is overlaid (circles). In Fig. 11 (c-d), if the variance for historical or
680 future periods lies outside the whiskers, we conclude an impact of the parametric effect on the
681 trends. However, if the variance across the 16 PPE members lies within the whiskers, we
682 conclude no impact of the parametric effect on the trend. Note that the variance in trends for
683 clear weather is in log-transformed space. As can be seen in Fig. 11c and 11d, the variance in
684 PPE trends for historical and future periods lies within the 95th percentile distribution of the

685 internal variability for both haze conducive and clear weather. Therefore, we do not find any
 686 discernible influence of the parametric effect on the trends in the frequencies.
 688



689

690
 691
 692

693 **Figure 11** Mean PPE trends for the frequency of (a) haze conducive weather (HWI>1) and (b)
 694 clear weather (HWI<-1) for winter. Circles show the mean trends from 16 PPE members for
 695 the historical (1979-2005) and near (2006-2032), mid (2033-2059) and far (2060-2086) future
 696 under the RCP8.5 scenario. Grey box and whiskers show the distribution of 10,000 values of
 697 trends sub-sampled from the control simulation. (c-d) same as (a-b) but mean is replaced by
 698 variance in trends. For box and whiskers, we first randomly sampled 10,000 time series of
 699 length 27 years using 2704 years of pre-industrial control simulation and calculated 10,000
 700 values of trends. We then randomly sub-sample 16 trends values from the 10,000 trend values
 701 and calculate the variance and mean of 16 trend values. The boxes are at the 25th and 75th
 702 percentile and the whiskers at 2.5th and 97.5th percentile of mean and variance distribution. For
 703 clear days, the frequencies were transformed to log space by applying a power transformation
 704 of $\log_{10}(1 + \text{frequency})$ before calculating trends.

705 **7. Conclusions**

706 In this study, we elucidate for the first time the influence of model physical
707 parametrisations, in addition to internal variability and climate change, on the future haze
708 conducive and clear weather conditions over the North China Plain (NCP) using the Perturbed
709 Parameter Ensemble (PPE) from the Met Office HadGEM3-GC3.05 model. We examine the
710 changes in winter (December-February) haze conducive and clear weather conditions for past
711 and future over the NCP using a large-scale meteorology-based daily Haze Weather Index
712 (HWI). We first identify the regional extent of the application of the HWI over China. We find
713 that the $HWI > 1$ can be used as an indicator of haze conducive weather conditions and $HWI < -$
714 1 as an indicator of clear weather conditions for the entire NCP due to the spatial coherence of
715 regional meteorological conditions over this region.

716 The PPE shows that under the RCP8.5 emission scenario, the mean frequency of haze
717 conducive weather ($HWI > 1$) can increase by up to ~65% in the near (2006-2032) and mid
718 (2033-2059) future and by ~87% in far future (2060-2086) as compared to the historical period
719 (1979-2005). In contrast, the frequency of clear weather ($HWI < -1$) can reduce by up to ~40%
720 in the near and mid-future and by ~57% in the far future. However, the opposite change of
721 relatively lower magnitude or negligible change in frequency of haze conducive and clear
722 weather, though less likely, is possible. The absolute number of days with haze conducive
723 weather in the far future can remain the same or up to ~3.5 times higher than the clear weather
724 over the NCP. There also exist a large interannual variability in the frequency of haze
725 conducive and clear weather conditions. However, no systematic change in the interannual
726 variance of the frequencies is noted in future as compared to the historical period. We also find
727 that enhanced vertical thermal stability due to the warming of the troposphere and weaker
728 northwesterlies over the NCP in the mid troposphere will collectively lead to more frequent
729 haze conducive weather over the NCP ~~the changes in the haze conducive weather ($HWI > 1$) for~~
730 ~~the future is associated with the changes in the mid-tropospheric zonal wind component and~~

731 ~~strong vertical temperature gradient between the lower to upper troposphere over the NCP.~~ We
732 find a consistently growing influence of anthropogenic climate change and parametric effect
733 on the mean haze conducive and clear weather frequencies across the 21st century. This
734 suggests that in addition to the internal variability, the parametric effect adds as an additional
735 source of uncertainty in future projections of haze conducive and clear weather, particularly
736 towards the end of the 21st century. We find that the impact of anthropogenic climate change
737 is discernible in trends for the historical period for haze conducive weather and up to mid of
738 the 21st century for clear weather. Beyond these periods, the historical trends are not sustained
739 and not distinguishable from the internal variability.

740 This study considers four atmospheric variables to examine the changes in future haze
741 conducive and clear weather conditions, however, other atmospheric variables (e.g., boundary
742 layer height) or processes may influence the occurrence of haze. Furthermore, even though our
743 study shows the potential for an increase in haze conducive weather conditions and a reduction
744 in clear weather conditions for the future periods, the actual formation of haze will depend on
745 future emissions of air pollutants and their precursors. If the source emissions are cut-off or
746 reduced in the future, the risk of haze formation would naturally reduce. Nevertheless, the
747 projections of changes in the frequency and interannual variance in haze conducive weather
748 conditions can be very useful for developing successful adaptation and mitigation policies for
749 the future that consider both emissions and climate change, and therefore can be beneficial for
750 near and long-term planning and decision-making in relation to improving future PM_{2.5} air
751 quality.

752 **Data Availability**

753 The Copernicus Climate Change Service (C3S) (2017): ERA5: Fifth generation of ECMWF
754 atmospheric reanalyses of the global climate data are available through Copernicus Climate

755 Change Service Climate Data Store (CDS) (<https://cds.climate.copernicus.eu/>). The PM2.5
756 concentrations for the US Embassy station in Beijing are archived at the following website
757 (<http://www.stateair.net/web/historical/1/1.html>). The haze weather index time series for PPE
758 and visibility data used in this paper can be obtained from the authors. The CAQRA dataset
759 can be freely downloaded at <https://doi.org/10.11922/sciencedb.00053>.

760 **Author Contribution**

761 SJ and RMD conceived and designed the manuscript; DS conducted PPE simulations using
762 Met Office HadGEM model; LP provided the visibility data; SJ performed data analysis,
763 produced figures, wrote the first draft; all co-authors provided comments on the manuscript
764 and contributed to writing.

765 **Competing interests**

766 The authors declare no financial or non-financial conflict of interest.

767 **Acknowledgements**

768 We thank Dr Li Ke for the discussion on the HWI calculation and Dr Peiqun Zhang for the
769 discussion on severe haze episodes in China. This work and its contributors (SJ, RMD, DS,
770 ST, ZS) were supported by the UK-China Research & Innovation Partnership Fund through
771 the Met Office Climate Science for Service Partnership (CSSP) China as part of
772 the Newton Fund (Met Office Reference Number: DN37368). RD and ZS also acknowledge
773 NERC for funding under the Atmospheric Pollution and Human Health Programme: Grant
774 Nos. NE/N006941/1 and NE/N007190/1. CL was supported by the National Key Research and
775 Development Program of China (Grant No. 2018YFA0606501). We also thank the two
776 reviewers for their constructive comments and suggestions on this manuscript.

777 **References**

778 An, Z., Huang, R. J., Zhang, R., Tie, X., Li, G., Cao, J., Zhou, W., Shi, Z., Han, Y., Gu, Z., and
779 Ji, Y.: Severe haze in northern China: A synergy of anthropogenic emissions and
780 atmospheric processes, *Proc Natl Acad Sci U S A*, 116, 8657-8666,
781 10.1073/pnas.1900125116, 2019.

782 Bai, N., Khazaei, M., van Eeden, S. F., and Laher, I.: The pharmacology of particulate matter
783 air pollution-induced cardiovascular dysfunction, *Pharmacology & therapeutics*, 113, 16-
784 29, 2007.

785 Cai, W., Li, K., Liao, H., Wang, H., and Wu, L.: Weather conditions conducive to Beijing
786 severe haze more frequent under climate change, *Nature Climate Change*, 7, 257-262,
787 10.1038/nclimate3249, 2017.

788 Callahan, C. W., Schnell, J. L., and Horton, D. E.: Multi-index attribution of extreme winter
789 air quality in Beijing, China, *Journal of Geophysical Research: Atmospheres*, 124, 4567-
790 4583, 2019.

791 Callahan, C. W., and Mankin, J. S.: The Influence of Internal Climate Variability on Projections
792 of Synoptically Driven Beijing Haze, *Geophysical Research Letters*, 47,
793 10.1029/2020gl088548, 2020.

794 Chen, H., and Wang, H.: Haze days in North China and the associated atmospheric circulations
795 based on daily visibility data from 1960 to 2012, *Journal of Geophysical Research:*
796 *Atmospheres*, 120, 5895-5909, 2015.

797 Deser, C., Knutti, R., Solomon, S., and Phillips, A. S.: Communication of the role of natural
798 variability in future North American climate, *Nature Climate Change*, 2, 775-779, 2012.

799 Deser, C., Phillips, A. S., Alexander, M. A., and Smoliak, B. V.: Projecting North American
800 climate over the next 50 years: Uncertainty due to internal variability, *Journal of Climate*,
801 27, 2271-2296, 2014.

802 Han, Z., Zhou, B., Xu, Y., Wu, J., and Shi, Y.: Projected changes in haze pollution potential in
803 China: an ensemble of regional climate model simulations, *Atmospheric Chemistry and*
804 *Physics*, 17, 10109-10123, 10.5194/acp-17-10109-2017, 2017.

805 Hawkins, E., and Sutton, R.: Time of emergence of climate signals, *Geophysical Research*
806 *Letters*, 39, n/a-n/a, 10.1029/2011gl050087, 2012.

807 He, J., Yu, Y., Xie, Y., Mao, H., Wu, L., Liu, N., and Zhao, S.: Numerical model-based
808 artificial neural network model and its application for quantifying impact factors of urban
809 air quality, *Water, Air, & Soil Pollution*, 227, 1-16, 2016.

810 Hersbach, H., Bell, B., Berrisford, P., Hirahara, S., Horányi, A., Muñoz-Sabater, J., Nicolas,
811 J., Peubey, C., Radu, R., Schepers, D., Simmons, A., Soci, C., Abdalla, S., Abellan, X.,
812 Balsamo, G., Bechtold, P., Biavati, G., Bidlot, J., Bonavita, M., Chiara, G., Dahlgren, P.,
813 Dee, D., Diamantakis, M., Dragani, R., Flemming, J., Forbes, R., Fuentes, M., Geer, A.,
814 Haimberger, L., Healy, S., Hogan, R. J., Hólm, E., Janisková, M., Keeley, S., Laloyaux,
815 P., Lopez, P., Lupu, C., Radnoti, G., Rosnay, P., Rozum, I., Vamborg, F., Villaume, S.,
816 and Thépaut, J. N.: The ERA5 global reanalysis, *Quarterly Journal of the Royal*
817 *Meteorological Society*, 146, 1999-2049, 10.1002/qj.3803, 2020.

818 Hong, C., Zhang, Q., Zhang, Y., Davis, S. J., Tong, D., Zheng, Y., Liu, Z., Guan, D., He, K.,
819 and Schellnhuber, H. J.: Impacts of climate change on future air quality and human health
820 in China, *Proceedings of the National Academy of Sciences*, 116, 17193-17200, 2019.

821 Hou, P., and Wu, S.: Long-term changes in extreme air pollution meteorology and the
822 implications for air quality, *Scientific reports*, 6, 1-9, 2016.

823 Jia, B., Wang, Y., Yao, Y., and Xie, Y.: A new indicator on the impact of large-scale circulation
824 on wintertime particulate matter pollution over China, *Atmospheric Chemistry and*
825 *Physics*, 15, 11919-11929, 2015.

826 Kan, H., London, S. J., Chen, G., Zhang, Y., Song, G., Zhao, N., Jiang, L., and Chen, B.:
827 Differentiating the effects of fine and coarse particles on daily mortality in Shanghai,
828 China, *Environment international*, 33, 376-384, 2007.

829 Kan, H., Chen, R., and Tong, S.: Ambient air pollution, climate change, and population health
830 in China, *Environment international*, 42, 10-19, 2012.

831 Kay, J. E., Deser, C., Phillips, A., Mai, A., Hannay, C., Strand, G., Arblaster, J. M., Bates, S.,
832 Danabasoglu, G., and Edwards, J.: The Community Earth System Model (CESM) large
833 ensemble project: A community resource for studying climate change in the presence of
834 internal climate variability, *Bulletin of the American Meteorological Society*, 96, 1333-
835 1349, 2015.

836 Knutti, R., Furrer, R., Tebaldi, C., Cermak, J., and Meehl, G. A.: Challenges in combining
837 projections from multiple climate models, *Journal of Climate*, 23, 2739-2758, 2010.

838 Kong, L., Tang, X., Zhu, J., Wang, Z., Li, J., Wu, H., Wu, Q., Chen, H., Zhu, L., and Wang,
839 W.: A 6-year-long (2013–2018) high-resolution air quality reanalysis dataset in China
840 based on the assimilation of surface observations from CNEMC, *Earth System Science*
841 *Data*, 13, 529-570, 2021.

842 Li, K., Liao, H., Cai, W., and Yang, Y.: Attribution of Anthropogenic Influence on
843 Atmospheric Patterns Conducive to Recent Most Severe Haze Over Eastern China,
844 *Geophysical Research Letters*, 45, 2072-2081, 10.1002/2017gl076570, 2018.

845 Li, Q., Zhang, R., and Wang, Y.: Interannual variation of the wintertime fog–haze days across
846 central and eastern China and its relation with East Asian winter monsoon, *International*
847 *Journal of Climatology*, 36, 346-354, 2016.

848 Liu, C., Zhang, F., Miao, L., Lei, Y., and Yang, Q.: Future haze events in Beijing, China: When
849 climate warms by 1.5 and 2.0°C, *International Journal of Climatology*, 40, 3689-3700,
850 10.1002/joc.6421, 2019.

851 Liu, Q., Jia, X., Quan, J., Li, J., Li, X., Wu, Y., Chen, D., Wang, Z., and Liu, Y.: New positive
852 feedback mechanism between boundary layer meteorology and secondary aerosol
853 formation during severe haze events, *Scientific reports*, 8, 1-8, 2018.

854 Liu, T., Gong, S., He, J., Yu, M., Wang, Q., Li, H., Liu, W., Zhang, J., Li, L., Wang, X., Li, S.,
855 Lu, Y., Du, H., Wang, Y., Zhou, C., Liu, H., and Zhao, Q.: Attributions of meteorological
856 and emission factors to the 2015 winter severe haze pollution episodes in China's Jing-
857 Jin-Ji area, *Atmospheric Chemistry and Physics*, 17, 2971-2980, 10.5194/acp-17-2971-
858 2017, 2017.

859 Pei, L., Yan, Z., Sun, Z., Miao, S., and Yao, Y.: Increasing persistent haze in Beijing: potential
860 impacts of weakening East Asian winter monsoons associated with northwestern Pacific
861 sea surface temperature trends, *Atmospheric Chemistry and Physics*, 18, 3173-3183,
862 2018.

863 Pendergrass, D., Shen, L., Jacob, D., and Mickley, L.: Predicting the impact of climate change
864 on severe wintertime particulate pollution events in Beijing using extreme value theory,
865 *Geophysical Research Letters*, 46, 1824-1830, 2019.

866 Petäjä, T., Järvi, L., Kerminen, V.-M., Ding, A., Sun, J., Nie, W., Kujansuu, J., Virkkula, A.,
867 Yang, X., and Fu, C.: Enhanced air pollution via aerosol-boundary layer feedback in
868 China, *Scientific reports*, 6, 1-6, 2016.

869 Qiu, L., Yue, X., Hua, W., and Lei, Y.-D.: Projection of weather potential for winter haze
870 episodes in Beijing by 1.5 °C and 2.0 °C global warming, *Advances in Climate Change*
871 *Research*, 11, 218-226, 10.1016/j.accre.2020.09.002, 2020.

872 Renhe, Z., Li, Q., and Zhang, R.: Meteorological conditions for the persistent severe fog and
873 haze event over eastern China in January 2013, *Science China Earth Sciences*, 57, 26-35,
874 2014.

875 Sexton, D. M., McSweeney, C. F., Rostron, J. W., Yamazaki, K., Booth, B. B., Murphy, J. M.,
876 Regayre, L., Johnson, J. S., and Karmalkar, A. V.: A perturbed parameter ensemble of
877 HadGEM3-GC3. 05 coupled model projections: part 1: selecting the parameter
878 combinations, *Climate Dynamics*, 56, 3395-3436, 2021.

879 Shen, L., Jacob, D. J., Mickley, L. J., Wang, Y., and Zhang, Q.: Insignificant effect of climate
880 change on winter haze pollution in Beijing, *Atmospheric Chemistry and Physics*, 18,
881 17489-17496, 10.5194/acp-18-17489-2018, 2018.

882 Sun, Y., Jiang, Q., Wang, Z., Fu, P., Li, J., Yang, T., and Yin, Y.: Investigation of the sources
883 and evolution processes of severe haze pollution in Beijing in January 2013, *Journal of*
884 *Geophysical Research: Atmospheres*, 119, 4380-4398, 2014.

885 Tie, X., Huang, R.-J., Cao, J., Zhang, Q., Cheng, Y., Su, H., Chang, D., Pöschl, U., Hoffmann,
886 T., and Dusek, U.: Severe pollution in China amplified by atmospheric moisture,
887 *Scientific Reports*, 7, 1-8, 2017.

888 Wang, J.-L., Zhang, Y.-h., Shao, M., Liu, X.-l., Zeng, L.-m., Cheng, C.-l., and Xu, X.-f.:
889 Quantitative relationship between visibility and mass concentration of PM_{2.5} in Beijing,
890 *Journal of environmental sciences*, 18, 475-481, 2006.

891 Wang, L., Wei, Z., Yang, J., Zhang, Y., Zhang, F., Su, J., Meng, C., and Zhang, Q.: The 2013
892 severe haze over southern Hebei, China: model evaluation, source apportionment, and
893 policy implications, *Atmospheric Chemistry and Physics*, 14, 3151-3173, 2014a.

894 Wang, Y., Yao, L., Wang, L., Liu, Z., Ji, D., Tang, G., Zhang, J., Sun, Y., Hu, B., and Xin, J.:
895 Mechanism for the formation of the January 2013 heavy haze pollution episode over
896 central and eastern China, *Science China Earth Sciences*, 57, 14-25, 2014b.

897 Xu, M., Chang, C. P., Fu, C., Qi, Y., Robock, A., Robinson, D., and Zhang, H. m.: Steady
898 decline of east Asian monsoon winds, 1969–2000: Evidence from direct ground
899 measurements of wind speed, *Journal of Geophysical Research: Atmospheres*, 111, 2006.

900 Xu, P., Chen, Y., and Ye, X.: Haze, air pollution, and health in China, *Lancet*, 382, 2067,
901 10.1016/S0140-6736(13)62693-8, 2013.

902 Yamazaki, K., Sexton, D. M., Rostron, J. W., McSweeney, C. F., Murphy, J. M., and Harris,
903 G. R.: A perturbed parameter ensemble of HadGEM3-GC3. 05 coupled model
904 projections: part 2: global performance and future changes, *Climate Dynamics*, 56, 3437-
905 3471, 2021.

906 Yin, Z., and Wang, H.: Role of atmospheric circulations in haze pollution in December 2016,
907 *Atmospheric Chemistry and Physics*, 17, 11673-11681, 10.5194/acp-17-11673-2017,
908 2017.

909 Zhang, Q., Ma, Q., Zhao, B., Liu, X., Wang, Y., Jia, B., and Zhang, X.: Winter haze over North
910 China Plain from 2009 to 2016: Influence of emission and meteorology, *Environ Pollut*,
911 242, 1308-1318, 10.1016/j.envpol.2018.08.019, 2018.

912 Zhang, R., Jing, J., Tao, J., Hsu, S.-C., Wang, G., Cao, J., Lee, C. S. L., Zhu, L., Chen, Z., and
913 Zhao, Y.: Chemical characterization and source apportionment of PM 2.5 in Beijing:
914 seasonal perspective, *Atmospheric Chemistry and Physics*, 13, 7053-7074, 2013.

915 Zhang, L., Wilcox, L. J., Dunstone, N. J., Paynter, D. J., Hu, S., Bollasina, M., ... & Zou, L.
916 (2021). Future changes in Beijing haze events under different anthropogenic aerosol
917 emission scenarios. *Atmospheric Chemistry and Physics*, 21(10), 7499-7514.

918 Zhang, Z., Gong, D., Mao, R., Kim, S. J., Xu, J., Zhao, X., and Ma, Z.: Cause and predictability
919 for the severe haze pollution in downtown Beijing in November-December 2015, *Sci*
920 *Total Environ*, 592, 627-638, 10.1016/j.scitotenv.2017.03.009, 2017.

921

922